Inorg. Chem. **2008**, *47*, 10009−10016

Temperature Driven Reactant Solubilization Synthesis of BiCuOSe

Evan S. Stampler,[†] William C. Sheets,[†,‡] Mariana I. Bertoni,[§] Wilfrid Prellier,[‡] Thomas O. Mason,[§] and Kenneth R. Poeppelmeier*[,†]

Department of Chemistry, Northwestern University, Evanston, Illinois 60208, Laboratoire CRISMAT, CNRS UMR 6508, ENSICAEN, 6 Blvd. Maréchal Juin, F-14050 Caen Cedex, France, and Department of Materials Science and Engineering, Northwestern University, Evanston, Illinois 60208

Received July 7, 2008

Phase-pure BiCuOSe, which is isostructural to the layered *p*-type transparent conductor LaCuOS, has been synthesized in high yield by a single-step hydrothermal reaction at low temperature (250 °C) and pressure (<20 atm). A moderate reaction temperature of 250 °C was sufficiently high to solubilize both Bi_2O_3 and Cu_2O and stabilize monovalent copper and low enough to impede the oxidation of dianionic selenium. BiCuOSe exhibits a relatively high electrical conductivity ($\sigma \approx 3.3$ S cm^{-1}) and a reduced band gap ($E_g = 0.75$ eV), which compare favorably with the optoelectronic properties of BiCuOS and the cerium-based oxysulfides, CeAgOS and CeCuOS.

Introduction

The quarternary rare-earth oxide chalcogenides have been studied extensively because of their potential applications as *p*-type transparent conductors. LaCuOS is a *p*-type conductor with an optically measured band gap of 3.1 eV.[1] The crystal structure of LaCuOS is shown in Figure 1. It belongs to a class of layered materials that adopts the ZrSiCuAs structure type in the tetragonal *P*4/*nmm* space group. The antifluorite $(Cu_2S_2)^{2-}$ chalcogenide layers, composed of slightly distorted edge-sharing CuS_4 tetrahedra, alternate with fluorite-like $(La_2O_2)^{2+}$ oxide layers, stacked perpendicular to the *c* axis of the tetragonal cell. Strong, covalent Cu−S bonds comprise the $(Cu_2S_2)^{2-}$ layers, while ionic La−O bonds comprise the $(La_2O_2)^{2+}$ layers, confining copper exclusively to the $(Cu_2S_2)^{2-}$ layers (i.e., copper is only bonded to sulfur). Owing to the reduced dimensionality of the $(Cu_2S_2)^{2-}$ layers, the valence band of LaCuOS is moderately dispersed leading to enhanced *p*-type conductivity.

The family of quarternary oxychalcogenides LnCuOQ (Ln = La−Ho and Y, Bi; Q = S, Se, Te) and oxide chalcogenides, in general, are synthesized by high temperature solid-state techniques. BiCuOSe has been synthesized previously by the direct reaction between stoichiometric amounts of Bi_2O_3 and elemental Bi, Cu, and Se in evacuated sealed quartz ampoules. The mixtures were initially heated at 400 °C for 48 h and finally annealed at 720 °C for 300 h.[2] A series of compounds of the form RE_2O_2Se (RE = La−Lu and Y, Bi) have been synthesized by reacting the appropriate

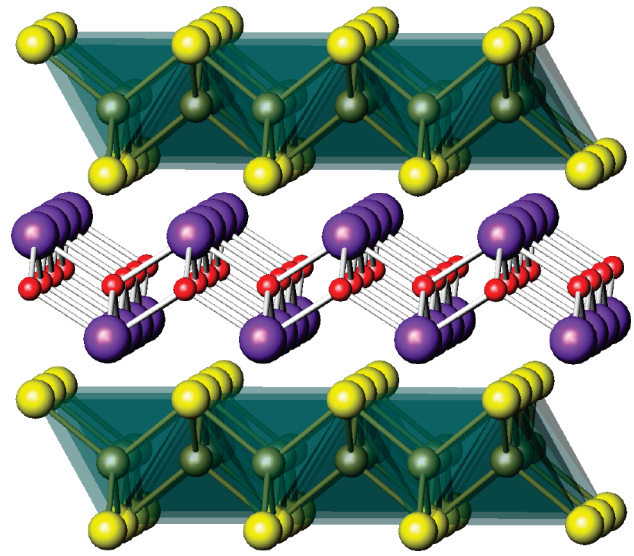

Figure 1. Schematic representation of the LaCuOS structure along the (100) axis, which is composed of $(La_2O_2)^{2+}$ and $(Cu_2S_2)^{2-}$ layers. For clarity, no La−S bonds are shown. Purple, gold, red, and yellow spheres represent La^{3+}, Cu^+, O^{2-}, and S^{2-} ions, respectively. Green polyhedra are used to define the edge-sharing CuS_4 tetrahedra.

* To whom correspondence should be addressed. E-mail: krp@northwestern.edu.
† Department of Chemistry, Northwestern University.
‡ Laboratoire CRISMAT, CNRS UMR 6508.
§ Department of Materials Science and Engineering, Northwestern University.

(1) Ueda, K.; Inoue, S.; Hirose, S.; Kawazoe, H.; Hosono, H. *Appl. Phys. Lett.* **2000**, *77* (77), 2701–2703.

10.1021/ic801267m CCC: $40.75
Published on Web 10/03/2008

sesquioxide with H_2Se at temperatures above 1000 °C.[3] While reports of high temperature preparations of oxide chalcogenides pervade the literature,[2,4−11] few examples of hydrothermally prepared oxide chalcogenides, and, in particular, oxide selenides exist. Heretofore the only oxide selenides that have been prepared by any solvothermal method belong to a series of compounds isotypic with the natural mineral cetineite, having the general formula $A_6[Sb_{12}O_{18}][SbX_3]_2 \cdot (6 - mx - y)H_2O \cdot x[B^{m+}(OH^-)_m] \cdot y\square$, where A = Na^+, K^+, Rb^+; X = S^{2-}, Se^{2-}; B = Na^+, Sb^{3+}; and □ may stand for an unoccupied lattice position. Owing to their interesting optical and electrical properties, these compounds, which form as subnanometer tubes arranged in a hexagonal rod packing, have drawn interest for their potential applications as chemical sensors or microlasers.[12−15] The synthesis of cetineite crystals involves a redox reaction between elemental antimony and the appropriate chalcogenide (S or Se) in a basic medium at temperatures below 250 °C.[16,17]

We recently expanded the list of hydrothermally prepared oxide chalcogenides with our report of the synthesis of BiCuOS via the direct reaction between Bi_2O_3, Cu_2O, and Na_2S at a reaction temperature of 250 °C.[18] We present here for the first time the low temperature (250 °C) and pressure (<20 atm) hydrothermal synthesis of BiCuOSe with a total reaction time of 48 h. The thermodynamics, Eh-pH (Pourbaix) and predominance diagrams are examined to understand how the reaction temperature affects speciation, solubility, and ultimately product formation. A reaction temperature of 250 °C solubilizes both Bi_2O_3 and Cu_2O and stabilizes monovalent copper species in solution, yet remains low enough to prevent selenide from oxidizing. Furthermore, the optical and electronic properties of BiCuOSe are experimentally and theoretically examined and compared to other layered oxychalcogenides, LnMOQ (Ln = La−Ho and Y, Bi; M = Cu, Ag; and Q = S, Se, Te), to understand the effect of varying the cationic and anionic species.

Experimental Section

Synthesis. Samples of polycrystalline BiCuOSe were prepared from the hydrothermal reaction between Bi_2O_3 (99.99%, Alfa Aesar), Cu_2O (99.9%, Alfa Aesar), and elementary Se (99.5+%, Aldrich). Stoichiometric amounts (1.30 mmol of Bi_2O_3 and Cu_2O, 2.60 mmol of Se; 1.0 g total mass) of these reagents were charged into a 125 mL poly(tetrafluoroethylene) (PTFE) Teflon-lined pressure vessel (Parr Instruments), which was then filled with 75 mL of distilled water and 1 mL of hydrazine hydrate (50−60%, Aldrich). The pressure vessel was then sealed and heated to 150 °C, followed by a controlled incremental temperature increase over 5 h to 250 °C. The maximum temperature was held constant for 48 h, followed by subsequent cooling to room temperature. The polycrystalline BiCuOSe products were recovered by filtration, followed by a deionized water rinse. The mass yield of the reaction is >80% (calculated on Bi). Samples of BiCuOS were prepared as described elsewhere.[18]

Powder X-ray Analysis. Powder X-ray diffraction (PXD) data were recorded on a Scintag XDS 2000 diffractometer operating at 40 kV and 20 mA with Ni-filtered Cu Kα radiation. Data were collected in the 10° to 80° 2θ range by pausing in 0.05° steps for 1 s. The PXD pattern of BiCuOSe was matched to JCPDS file 45-0296 using the Jade software suite.[19] The experimental powder data were also matched to a calculated PXD patterns generated from published crystallographic data by the PowderCell software suite.[20]

Inductively Coupled Plasma (ICP) Spectrometry. A VISTA-MPX CCD Simultaneous Varian ICP Spectrometer was used to measure the molar ratio of Bi/Cu for BiCuOSe. Approximately 0.0050 g of BiCuOSe was dissolved in 3 mL of HNO_3 by heating the mixture at 55 °C for 3 h, and the solution was diluted to a measurable concentration (ppm) with Milli-Q water. The cationic Bi/Cu ratio in hydrothermally prepared powders of BiCuOSe was determined to be 1.00/0.98, within the limit of accuracy of the ICP spectrometer. Measurements were performed in triplicate to ensure a high degree of accuracy.

Electron Microscopic Analysis. Electron microscopy studies of BiCuOSe were carried out using a Hitachi S-4500 scanning electron microscope (SEM). To prepare SEM samples, polycrystalline samples were attached to an aluminum mount using carbon tape and then coated with 5 nm gold. Energy-dispersive X-ray (EDX) analysis (Hitachi S-3500 SEM) was used to analyze the stoichiometry of the sample. Analysis confirmed the samples to have an ionic ratio of 1.00/0.97/1.00 for Bi/Cu/Se, within the limit of accuracy of the EDX technique; oxygen was observed but not quantified (see Figure S1 in the Supporting Information).

Optical Analysis. Optical data were obtained via diffuse reflectance. In a diffuse reflectance experiment, the nonspecular component of reflection (i.e., radiation that has undergone multiple scattering events on different particles and returned to the sample

(2) Kusainova, A. M.; Berdonosov, P. S.; Akselrud, L. G.; Kholodkovskaya, L. N.; Dolgikh, V. A.; Popovkin, B. A. *J. Solid State Chem.* **1994**, *112* (112), 189–191.
(3) Guittard, M.; Flahaut, J.; Domange, L. *Acta Crystallogr.* **1966**, *21* (21), 832.
(4) Berdonosov, P. S.; Kusainova, A. M.; Kholodkovskaya, L. N.; Dolgikh, V. A.; Akselrud, L. G.; Popovkin, B. A. *J. Solid State Chem.* **1995**, *118* (118), 74–77.
(5) Chan, G. H.; Deng, B.; Bertoni, M.; Ireland, J. R.; Hersam, M. C.; Mason, T. O.; Van Duyne, R. P.; Ibers, J. A. *Inorg. Chem.* **2006**, *45* (45), 8264–8272.
(6) Huang, F. Q.; Brazis, P.; Kannewurf, C. R.; Ibers, J. A. *J. Solid State Chem.* **2000**, *155* (155), 366–371.
(7) Ijjaali, I.; Haynes, C. L.; McFarland, A. D.; Van Duyne, R. P.; Ibers, J. A. *J. Solid State Chem.* **2003**, *172* (172), 257–260.
(8) Liu, M. L.; Wu, L. B.; Huang, F. Q.; Chen, L. D.; Ibers, J. A. *J. Solid State Chem.* **2007**, *180* (180), 62–69.
(9) Popovkin, B. A.; Kusainova, A. M.; Dolgikh, V. A.; Aksel'rud, L. G. *Zh. Neorg. Khim.* **1998**, *43* (43), 1589–1593.
(10) Ueda, K.; Takafuji, K.; Hiramatsu, H.; Ohta, H.; Kamiya, T.; Hirano, M.; Hosono, H. *Chem. Mater.* **2003**, *15* (15), 3692–3695.
(11) Ueda, K.; Hirose, S.; Kawazoe, H.; Hosono, H. *Chem. Mater.* **2001**, *13* (13), 1880–1883.
(12) Simon, U.; Jockel, J.; Starrost, F.; Krasovskii, E. E.; Schattke, W. *Nanostruct. Mater.* **1999**, *12* (12), 447–450.
(13) Simon, U.; Schuth, F.; Schunk, S.; Wang, X. Q.; Liebau, F. *Angew. Chem., Int. Ed. Engl.* **1997**, *36* (36), 1121–1124.
(14) Starrost, F.; Krasovskii, E. E.; Schattke, W.; Jockel, J.; Simon, U.; Adelung, R.; Kipp, L. *Phys. Rev. B: Condens. Matter* **2000**, *61* (61), 15697–15706.
(15) Starrost, F.; Krasovskii, E. E.; Schattke, W.; Jockel, J.; Simon, U.; Wang, X.; Liebau, F. *Phys. Rev. Lett.* **1998**, *80* (80), 3316–3319.
(16) Wang, X.; Liebau, F. *Eur. J. Solid State Inorg. Chem.* **1998**, *35* (35), 27–37.
(17) Wang, X.; Liebau, F. *Z. Kristallogr.* **1999**, *214* (214), 820–834.
(18) Sheets, W. C.; Stampler, E. S.; Kabbour, H.; Bertoni, M. I.; Cario, L.; Mason, T. O.; Marks, T. J.; Poeppelmeier, K. R. *Inorg. Chem.* **2007**, *46* (46), 10741–10748.
(19) *Jade*, 5.0; Materials Data Inc.: Livermore, CA, 1999.
(20) *PowderCell*, 2.4; Federal Institute for Materials Research and Testing: Berlin, Germany, 2000.

surface) is measured relative to a standard.[21] Diffuse reflectance data were collected over the spectral range 200 nm (6.2 eV) to 2600 nm (0.48 eV) using a Varian Cary 5000 UV/vis/NIR scanning double beam spectrophotometer equipped with an integrating sphere (110 mm in diameter; Cary 1E with Cary 1/3 attachment, Varian Walnut Creek, CA). Baseline spectra were collected on pressed PTFE Halon placed in the sample and reference beams. Data were collected with a scan rate of 150 nm min^{-1}, a data interval of 0.5 nm, an average step time of 0.2 s, and a signal bandwidth of 3 nm. Pellets of BiCuOSe and BiCuOS were mounted on a blackened sample mask. The reflectance data were translated into absorption data (α/S) by using an equation developed by Kubelka and Munk, $\alpha/S = (1 - R)^2/2R$, where α is the absorption coefficient, S is the scattering coefficient, and R is the diffuse reflectance at a certain energy.[22]

Electrical Measurements. The as-prepared polycrystalline sample of BiCuOSe was pressed into a pellet (0.5″ dia.) using a cold isostatic press. Owing to the instability of oxide chalcogenides in air at elevated temperatures, the pellet was sealed in an evacuated silica−glass ampule and sintered at 720 °C for 48 h. In preparation for electrical measurements, a bar (∼ 2 mm × 2 mm × 13 mm) was cut from the sintered disk using an abrasive slurry disk cutter. The electrical conductivity of the sample was obtained by a 4-probe method from 5−300 K using a Quantum Design physical property measurement system (PPMS). Electrical contacts consisted of fine gold wire attached to the bars with ultrasonically deposited indium paste. Thermopower measurements were made using a steady-state technique with a small temperature gradient of ∼1 K/cm detected by a chromel-constantan thermocouple from 5 to 300 K in a liquid He cryostat.

Electronic Structure Calculations. Linear Muffin-Tin Orbital (LMTO) calculations[23,24] on BiCuOSe and BiCuOS were performed within the atomic sphere approximation using version 47C of the Stuttgart TB-LMTO-ASA program.[25] Scalar-relativistic Kohn−Sham equations within the local density approximation[26] were solved taking all relativistic effects into account except for the spin−orbit coupling. The calculations were performed on 484 irreducible k points within the primitive wedge of the Brillouin zone. Calculations were performed on the refined crystal structures of BiCuOSe (space group $P4/nmm$, $a = 3.921$ Å, $c = 8.913$ Å)[2] and BiCuOS (space group $P4/nmm$, $a = 3.871$ Å, $c = 8.561$ Å).[9] These calculations permitted plots of the electron localization function (ELF) to be made, which when plotted in the real space of the crystal structure enables visualization of the lone pairs.

Results and Discussion

Knowledge of the dominant species in solution at a certain pH, temperature, pressure, and oxidation potential enables interpretation of the solubility of reagents in aqueous solutions.[27] Such experimental information is essential to understanding and anticipating what products can form under the autogenous conditions generated in hydrothermal pressure vessels.[27−30]

Insight into the dominant species of the Ln_2O_3−H_2O system at different temperatures reveals the difficulties associated with the hydrothermal preparation of lanthanide copper oxide selenides, LnCuOSe (Ln = La−Ho). The speciation and therefore reactivity of rare-earth oxides in aqueous solution is almost entirely temperature dependent. At room temperature the solubility of rare-earth oxides, Ln_2O_3, in aqueous solutions is negligible.[31] Instead, rare-earth oxides hydrolyze to generate the insoluble rare-earth hydroxide, $Ln(OH)_3$. Owing to the reduced dielectric constant and related reduction in shielding of Ln^{3+} ions by surrounding aquo ligands, the extent of rare-earth hydroxide dissolution increases at elevated temperatures. Additionally, via a temperature driven decomposition, the rare-earth hydroxide releases water to form the more soluble and reactive rare-earth oxide hydroxide, LnO(OH). At ambient temperatures, the insoluble and solid rare-earth hydroxide persists. With increasing temperature the rare-earth hydroxide slowly dehydrates to the more reactive rare-earth oxide hydroxide, the transition proceeding at lower temperatures with an increase in atomic number ($T_{Yb} \approx 140$ °C; $T_{Lu} \approx 100$ °C).[32] Such a trend results from the decrease in rare-earth oxide basicity upon proceeding from lanthanum oxide to lutetium oxide, as would be expected from the decrease in the rare-earth cation atomic radius.[32−35] Because of the exceedingly high dehydration temperature of $La(OH)_3$ (∼ 800 °C)[32] and the inherent temperature limitations of Teflon-lined pressure vessels (250 °C), attempts to prepare LaCuOSe resulted in unreacted $La(OH)_3$. LnCuOSe containing lanthanides (Ln = Er−Lu) with a transition temperature compatible with hydrothermal conditions does not overlap with the known stable phases. The commensurability of the $(Ln_2O_2)^{2+}$ and $(Cu_2Se_2)^{2-}$ layers is maintained by equal contraction or extension of both unshared edges of the hypothetical $CuSe_4$ tetrahedra. For the selenium series the smallest rare-earth ion to form this structure is holmium, at which point the $CuSe_4$ tetrahedra reach their distortion limit and the smallest Cu−Cu distance is observed. The dehydration temperature of $Ho(OH)_3$ to the more reactive rare-earth oxide hydroxide is still above the limitations of Teflon-lined pressure vessels; thus, the hydrothermal synthesis of rare-earth copper oxide selenides was not observed.

The synthesis of phase-pure samples of BiCuOSe was facilitated by the aqueous chemistry of Bi_2O_3 and Cu_2O.

(21) Hecht, H. G. *Mod. Aspects Reflectance Spectrosc., Proc. Symp., Chicago* **1968**, 1–26.
(22) Kubelka, P.; Munk, F. *Z. Tech. Phys. (Leipzig)* **1931**, *12* (12), 593.
(23) Andersen, O. K. *Phys. Rev. B: Solid State* **1975**, *12* (12), 3060–3083.
(24) Jepsen, O.; Andersen, O. K. *Z. Phys. B.: Condens. Matter* **1995**, *97* (97), 35–47.
(25) Jepsen, O.; Andersen, O. K. *The Stuttgart TB-LMTO-ASA Program*, version 47; MPI fur Festkorperforschung: Stuttgart, Germany, 2000.
(26) Von Barth, U.; Hedin, L. *J. Phys. C: Solid State Phys.* **1972**, *5* (5), 1629–1642.
(27) Rabenau, A. *Angew. Chem., Int. Ed. Engl.* **1985**, *24* (24), 1026–1040, and references therein.
(28) Sheets, W. C.; Mugnier, E.; Barnabe, A.; Marks, T. J.; Poeppelmeier, K. R. *Chem. Mater.* **2006**, *18* (18), 7–20.
(29) Walton, R. I. *Chem. Soc. Rev.* **2002**, *31* (31), 230–238.
(30) Whittingham, M. S.; Guo, J.-D.; Chen, R.; Chirayil, T.; Janauer, G.; Zavalij, P. *Solid State Ionics* **1995**, *75* (75), 257–268.
(31) Deberdt, S.; Castet, S.; Dandurand, J.-L.; Harrichoury, J.-C.; Louiset, I. *Chem. Geol.* **1998**, *151* (151), 349–372.
(32) Klevtsov, P. V.; Sheina, L. P. *Neorg. Mater.* **1965**, *1* (1), 912–917.
(33) Shafer, M. W.; Roy, R. *Z. Anorg. Allg. Chem.* **1954**, *276* (276), 275–288.
(34) Viswanathiah, M. N.; Tareen, J. A. K.; Kutty, T. R. N. *Mater. Res. Bull.* **1980**, *15* (15), 855–859.
(35) Yamamoto, O.; Takeda, Y.; Kanno, R.; Fushimi, M. *Solid State Ionics* **1985**, *17* (17), 107–114.

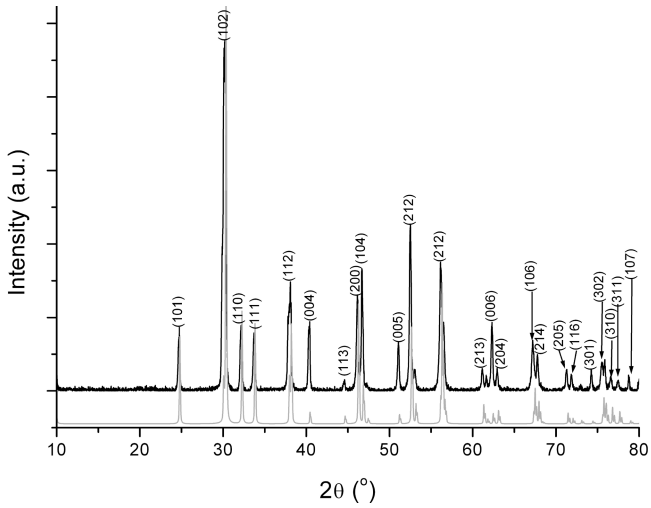

Figure 2. PXD pattern of the BiCuOSe product. Calculated positions, both indexed and indicating relative intensities, are shown in gray for BiCuOSe.

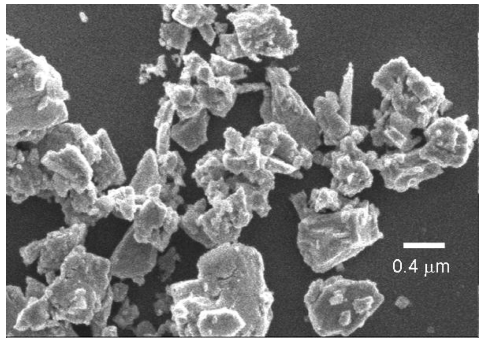

Figure 3. SEM image of BiCuOSe crystallites ranging in size from a few tenths of a micrometer up to ~1 μm.

While the high basicity of the oxides of the large rare-earths precluded the synthesis of LnCuOSe, the aqueous chemistry of bismuth and copper were conducive to the synthesis of BiCuOSe. Phase-pure BiCuOSe is prepared on a gram scale in 48 h, which is significantly less than the 300 h required in evacuated sealed tube preparations.[4,9] The phase purity of samples was verified by PXD and a representative pattern is shown in Figure 2. The pattern can be indexed to BiCuOSe (JCPDS 45-0296, $a = 3.921$ Å, $c = 8.913$ Å, space group *P*4/*nmm*) with a tetragonal unit cell. The unit cell parameters are in good agreement with previous reports.[2] As illustrated by the SEM image in Figure 3, crystallite sizes of the hydrothermally prepared BiCuOSe samples range from a few tenths of a micrometer to 1 μm.

In contrast to rare-earth oxides, the oxides of bismuth exhibit acid/base character ranging from acidic to amphoteric. Trivalent bismuth persists in aqueous solution at all pHs except under strongly oxidizing conditions with the stability domain of pentavalent bismuth in the Eh-pH diagram lying well above the oxidation potential of water. At 300 °C Bi_2O_3 exhibits a maximum molar solubility of 10^{-3},[36,37] a substantial increase over its room temperature solubility of 10^{-5} M.[38] Similarly, the solubility of Cu_2O scales with temperature and achieves a maximum molar solubility of $[Cu^+] \approx 10^{-4}$ at 200 °C, an order of magnitude greater than at 150 °C.[39−41] While Cu_2O disproportionates to copper metal and soluble Cu^{2+} species in aqueous solution at room temperature, the stability area of the Cu^+ ion increases with increasing temperature. The dielectric constant of water decreases with rising temperature and increases with rising pressure, the temperature effect predominating,[27] which destabilizes the more highly charged Cu^{2+} ion and lowers the impetus for disproportionation.[39,42] Elevated temperature facilitated the solubilization of Bi_2O_3 and Cu_2O and also stabilized monovalent copper.

While generation of the soluble bismuth and copper species was achieved by raising the reaction temperature, the desired water-soluble selenium species were generated via a direct redox reaction between hydrazine and elemental selenium. The typical oxidation products of hydrazine are nitrogen gas and water; an advantage over other reducing agents (e.g., $LiAlH_4$, $K_3Fe(CN)_6$), etc.) that include corresponding cations which can potentially incorporate themselves into the reaction. Careful consideration was given to determine the proper pH and temperature where soluble dianionic selenium species predominate. To avoid oxidation of the selenide anion, neutral or basic solutions are preferred in the preparation of metal selenides.[43] However, selenium hydrolyzes in alkaline solutions so neutral conditions were targeted.[27] The Se−H_2O Pourbaix (Eh-pH) diagram plotted for 25 °C reveals that HSe^- ions are the dominant selenium species in solution above pH = 4.[43] The stability domain of this species reaches a few tenths of a volt above the reduction potential of water, minimizing the impetus for oxidation to the highly stable complex oxoanionic SeO_4^{2-}, SeO_3^{2-}, and $HSeO_3^-$ species. The size of the stability field of HSe^- scales inversely with temperature with its upper stability line lying less than a tenth of a volt above the reduction potential of water at 300 °C and the insoluble H_2Se predominating up to pH = 7.0.[43] A reaction temperature of 250 °C was high enough to solubilize Bi_2O_3 and Cu_2O and, at the same time, low enough that the stability field of HSe^- lay above the oxidation potential of water at neutral pH.

The selenium species identified above do not account for the presence of the copper ions. In solution selenium complexes with copper to form Cu−Se species, an association that cooperatively increases both ions' solubility. While the solubility of copper is enhanced through complexation with selenium, the exact copper−selenium species that exist in solution are not known.[44] The aqueous copper−sulfur species have been studied more extensively and because

(36) Kolonin, G. R.; Laptev, Y. V. *Geokhimiya* **1982**, 1621–1631.
(37) Laptev, Y. V.; Kolonin, G. R. *Zh. Neorg. Khim.* **1982**, *27* (27), 2515–2520.
(38) Baes, C. F., Jr.; Mesmer, R. E. *The Hydrolysis of Cations*; Krieger Publishing Company: Malabar, FL, 1976.
(39) Beverskog, B.; Puigdomenech, I. *J. Electrochem. Soc.* **1997**, *144* (144), 3476–3483.
(40) Var'yash, L. N.; Rekharskii, V. I. *Geokhimiya* **1981**, 1003–1008.
(41) Var'yash, L. N.; Rekharskii, V. I. *Geokhimiya* **1981**, 683–688.
(42) Var'yash, L. N. *Geokhimiya* **1991**, 1066–1074.
(43) D'Yachkova, I. B.; Khodakovskii, I. L. *Geokhimiya* **1968**, 1358–1375.
(44) Sagindykova, Z. B.; Shalaeva, T. S.; Semina, O. I.; Khim.-Metal. Inst., Karaganda, U.S.S.R., **1981**.

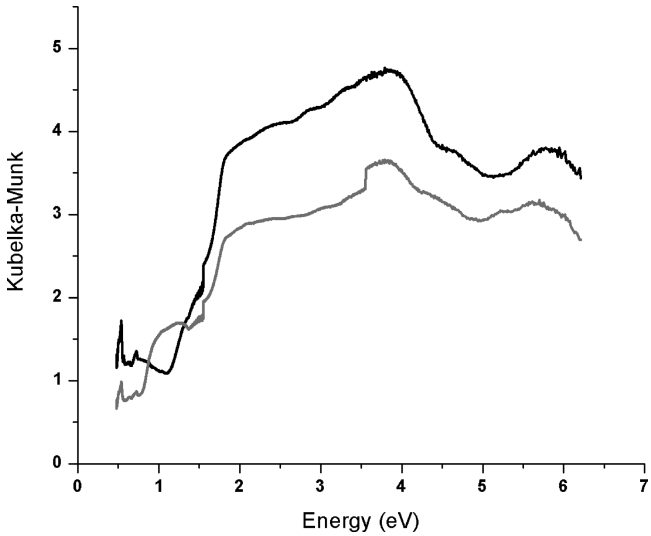

Figure 4. Kubelka−Munk absorption spectra of as-prepared BiCuOSe (black) and BiCuOS (gray) with respect to a PTFE Halon standard.

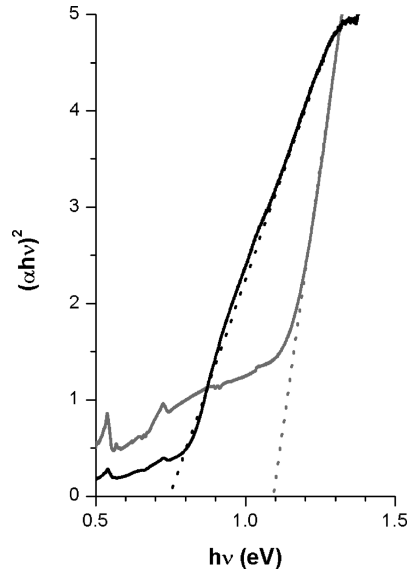

Figure 5. $(\alpha h\nu)^2$ vs $h\nu$ plot for BiCuOSe (black) and BiCuOS (gray). The dotted lines estimate the band gaps of the respective material.

selenium resembles sulfur in both its chemical reactivity[45] and its behavior in aqueous solutions, the Eh-pH diagrams for such species can be used as a guide.[38] The sulfur and selenium Eh-pH diagrams are qualitatively very similar with both showing that HS^- and HSe^- species predominate in solution.[43,46,47] A cumulative Pourbaix diagram detailing the Cu−S−H_2O system shows that through the interaction of copper and sulfur in solution, the copper thio-complex, $Cu(HS)_2^-$, predominates in neutral conditions.[48] All things considered, it is likely that a similar $Cu(HSe)_2^-$ species is present in the Cu−Se−H_2O system under the same conditions.

The optical properties of BiCuOSe and BiCuOS were studied using diffuse reflectance spectroscopy. Spectra collected from 200−2600 nm (Figure 4) reveal that BiCuOSe and BiCuOS absorb light across the entire visible range (1.65−3.1 eV), which is consistent with their black color. As depicted in Figure 5, the derived optical band gaps of BiCuOSe (∼0.75 eV) and BiCuOS (∼1.09 eV) compare favorably, both being considerably smaller than those of the isostructural rare-earth oxychalcogenides (e.g., 3.1 eV for LaCuOS[1]). The projected density of states (DOS) and LMTO calculated band structures of BiCuOSe and BiCuOS are depicted in Figures 6 and 7, respectively. The DOS of BiCuOSe and BiCuOS are qualitatively very similar. The small optical band gaps of BiCuOSe and BiCuOS result from the contribution to the conduction band minimum (CBM) of low energy bismuth 6p orbitals that lie a few tenths of an electronvolt above the valence band maximum (VBM). In BiCuOSe the CBM is located at the Γ point, whereas the VBM is located between the M and Γ points. The indirect band gap is nearly zero and similar to CeAgOS, transitions between these points of different symmetries are weak or

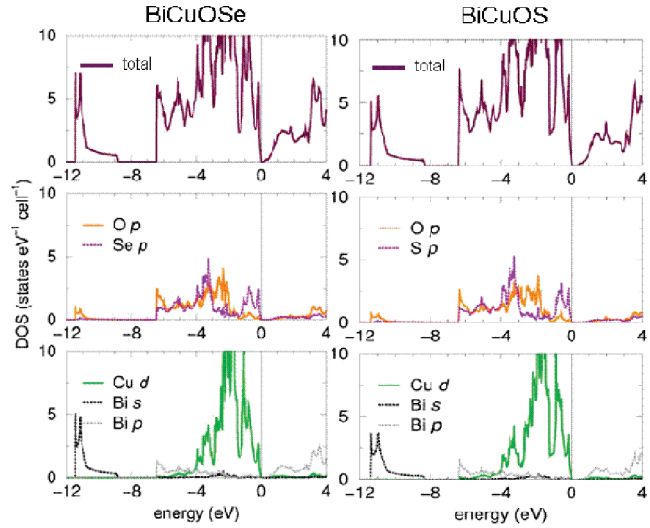

Figure 6. Projected LMTO densities of states (DOS), with each atomic contribution highlighted in color, for BiCuOSe (left) and BiCuOS (right). In this plot, the top of the valence band is taken as zero on the energy axis.

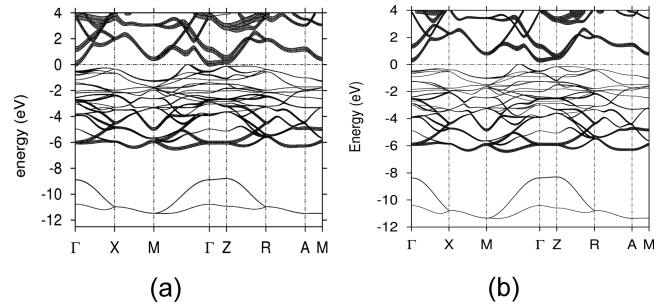

Figure 7. Calculated band structures for (a) BiCuOSe Bi p-states, (b) BiCuOS Bi p-states. The fatbands show the respective orbital contribution to the band structure. In this plot, the top of the valence band is taken as zero on the energy axis.

forbidden. Hence, we assign a calculated direct band gap of 0.15 eV at the next lowest energy, the Z point, for BiCuOSe. The calculated direct band gap of BiCuOS at Z is 0.50 eV.[18] It should be noted that the LDA calculated band gaps are

(45) Huston, D. L.; Sie, S. H.; Suter, G. F.; Cooke, D. R.; Both, R. A. *Econ. Geol. Bull. Soc. Econ. Geol.* **1995**, *90* (90), 1167–1196.
(46) Campbell, J. A.; Whiteker, R. A. *J. Chem. Educ.* **1969**, *46* (46), 90–92.
(47) Murray, R. C., Jr.; Cubicciotti, D. *J. Electrochem. Soc.* **1983**, *130* (130), 866–869.
(48) Young, C. A.; Dahlgren, E. J.; Robins, R. G. *Hydrometallurgy* **2003**, *68* (68), 23–31.

consistently underestimated by approximately 0.5−2.0 eV, a level of discrepancy which is not unusual for oxides.[49] The systematic error is expected to cancel, however, because we focus on the difference between band gaps within a group of similar compounds. The difference in the calculated band gaps of BiCuOSe and BiCuOS (0.45 eV) compares well with the experimentally determined value of 0.34 eV.

The small band gaps of bismuth-based materials are a result of the low energy of bismuth 6p orbitals which is attributed to scalar relativistic effects often associated with sixth row elements. Despite having similar orbital contributions to its VBM as BiCuOSe and BiCuOS, LaCuOS has a substantially larger band gap. The CBM of LaCuOS is composed of copper 4s and lanthanum 5d states at a much higher energy and therefore exhibits a much larger band gap, highlighting the role of scalar relativistic effects in reducing the band gaps of bismuth copper oxide chalcogenides.[18] LMTO calculations on a series of bismuthates ($NaBiO_3$, $MgBi_2O_6$, $SrBi_2O_6$, $BaBi_2O_6$, and $ZnBi_2O_6$) conclude that scalar relativistic effects lower the energy level and decrease the spatial extent of the CBM, which comprise the empty bismuth 6s orbitals.[50] Both of these changes reduce the bismuth 6s to oxygen 2p overlap, decreasing the antibonding character and thereby substantially lowering its energy level. The CBM of BiCuOSe is composed primarily of bismuth 6p states and not bismuth 6s states as in the previously discussed bismuthates. Bismuth is formally Bi^{5+} in the bismuthates and formally Bi^{3+} in BiCuOSe. Similar to other bismuth oxides with bismuth in a formal Bi^{3+} oxidation state, the filled bismuth 6s states contribute primarily in a window of energy 8−12 eV below the VBM.[51,52] Nevertheless, scalar relativistic effects play a similar role in lowering the energy of bismuth 6p states, albeit to a lesser extent than bismuth 6s states,[53] and therefore the CBM in the oxychalcogenides. Regardless of oxidation state, owing to relativistic effects associated with sixth row elements, designing transparent conductors based on bismuth is difficult.

Because the CBMs of both BiCuOSe and BiCuOS comprise mainly bismuth 6p states, little difference was expected in their CBMs. Instead, the CBM rises in energy by approximately 0.1 eV upon substituting sulfur for selenium. In BiCuOS upon moving from Γ to Z the band bends upward, while this region is essentially flat in BiCuOSe. This band bending in conjunction with the upward shift of the CBM results in the conduction band at Z in BiCuOS being slightly higher in energy than in BiCuOSe (Figure 8), which, in agreement with the experimentally observed band gaps, leads to a calculated band gap a few tenths of an electronvolt larger in BiCuOS.

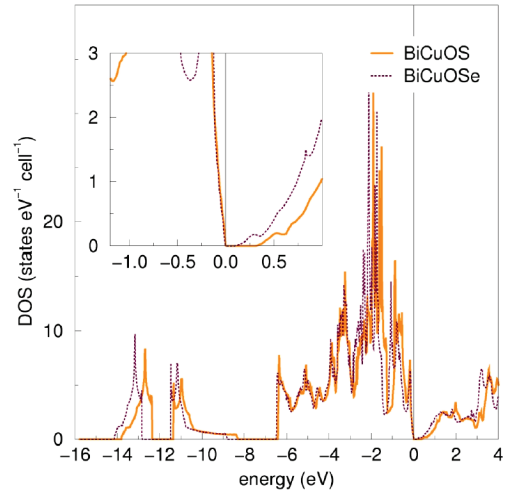

Figure 8. Projected LMTO DOS of BiCuOSe (purple dashed line) and BiCuOS (orange line). The inset zooms in on the CBMs of the respective materials between 0 and 0.5 eV. In this plot, the top of the valence band is taken as zero on the energy axis.

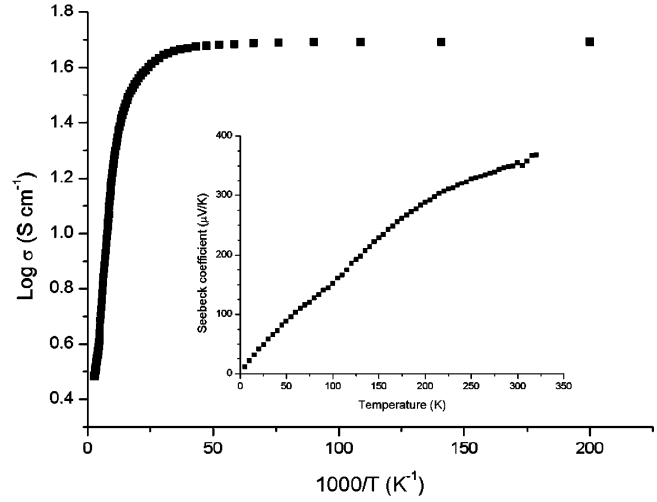

Figure 9. Temperature dependence of electrical conductivity (σ) in BiCuOSe. The inset of the figure shows the temperature dependence of the Seebeck coefficient of BiCuOSe.

Thermoelectric power measurements were performed on a sintered bar (∼ 2 mm × 2 mm × 13 mm) of BiCuOSe (Figure 9). Similar to other layered rare-earth oxide chalcogenides, BiCuOSe has a positive Seebeck coefficient of ∼ 350 μV/K at room temperature, indicating that it is a *p*-type semiconductor. The primary origin of hole carriers is most likely Cu^+ vacancies. Indeed, Ohtani et al. show that the conductivity of $BiCu_{1-x}OSe$ ($0 \geq x \geq 0.020$) prepared by solid state techniques increases as x increases, indicating such a mechanism for hole generation.[54] ICP and EDX measurements indicate that hydrothermally prepared samples of BiCuOSe have Cu^+ vacancies with $x \approx 0.02$. The off-stoichiometry between bismuth and copper presumably results from the slightly lower aqueous solubility of copper. Figure 9 reveals that hydrothermally prepared BiCuOSe has a room temperature conductivity of ∼3.3 S cm^{-1}, equivalent to that of $BiCu_{0.98}OSe$ prepared by solid state techniques.[54]

(49) Eng, H. W.; Barnes, P. W.; Auer, B. M.; Woodward, P. M. *J. Solid State Chem.* **2003**, *175* (175), 94–109.
(50) Mizoguchi, H.; Woodward, P. M. *Chem. Mater.* **2004**, *16* (16), 5233–5248.
(51) Payne, D. J.; Egdell, R. G.; Walsh, A.; Watson, G. W.; Guo, J.; Glans, P. A.; Learmonth, T.; Smith, K. E. *Phys. Rev. Lett.* **2006**, *96* (96), 157403/157401−157403/157404.
(52) Seshadri, R. *Solid State Sci.* **2006**, *8* (8), 259–266.
(53) *Inorganic Chemistry*, 1st ed.; Wiberg, N., Holleman, A. F., Wiberg, E., Eds.; Academic Press: New York, 2001.
(54) Ohtani, T.; Tachibana, Y.; Fujii, Y. *J. Alloys Compd.* **1997**, *262−263* (262−263), 175–179.

The room temperature conductivity of hydrothermally prepared BiCuOS is reported to be 0.08 S cm^{-1}.[18] Additional reports on the direct solid state synthesis of BiCuOQ (Q = S or Se)[55] reveal that the conductivities of samples synthesized hydrothermally are consistently higher, indicating that the hydrothermal method represents a unique route toward the preparation of materials with improved electrical properties.

The conductivities of hydrothermally prepared samples of both BiCuOSe and BiCuOS are substantially higher than previous reports of the isostructural LnCuOS (Ln = La, Pr, and Nd). Sintered pressed pellets of LaCuOS, PrCuOS, and NdCuOS powders are reported to have conductivities of 8.0×10^{-6} S/cm, 1.6×10^{-5} S/cm, and 3.8×10^{-4} S/cm, respectively.[10] While the VBMs of BiCuOSe and BiCuOS are qualitatively similar from −3 to 0 eV, Figure 8 reveals that the states at the top of the valence band of BiCuOSe are slightly more dispersed. Owing to a better energy match between copper 3d and selenium 4p orbitals, increased orbital mixing leads to a higher hole mobility in the copper−selenium manifold. Similarly, substituting selenium for sulfur in LaCuOQ (Q = S, Se) enhances dispersion of the valence band near the Fermi level and a related higher mobility in LaCuOSe (8.0 cm^2 V^{-1} s^{-1}) compared to LaCuOS (0.5 cm^2 V^{-1} s^{-1}) is observed.[56] The higher hole mobilities are reflected in the conductivities as systematic substitution of selenium for sulfur in nondoped $LaCuOS_{1-x}Se_x$ ($0 \le x \le 1$) results in a concomitant rise in room temperature conductivity (10^{-6} S $cm^{-1} \le \sigma \le 10^{-3}$ S cm^{-1}), while maintaining a similar band gap energy.[57,58] The valence bands of BiCuOSe and LaCuOSe are qualitatively very similar, both resulting from strong overlap between Cu 3d and Se 4p orbitals in the $(Cu_2Se_2)^{2-}$ layers, but the conductivity of BiCuOSe is a few orders of magnitude greater than that of LaCuOSe.[59] The conductivity of BiCuOSe compares more favorably with that of Sr-doped powder samples of LnCuOS (Ln = La, Pr, Nd),[10] CeAgOS (0.16 S/cm),[5] and CeCuOS (0.61 S/cm).[10] The higher conductivity of the cerium-based oxysulfides has been ascribed to both ionic (CeAgOS) and semimetallic (CeCuOS) conduction mechanisms. Ueda et al. consider CeCuOS to be in a semimetallic state, as ultraviolet and inverse photoemission spectroscopy measurements reveal the presence of an unoccupied band near the Fermi level.[10] Considering that BiCuOSe has a low energy lying CBM near the Fermi level composed of unoccupied Bi 6p orbitals, the unique optical and electrical transport properties of BiCuOSe are more characteristic of a semimetallic state.

The electronic properties of semiconductors, such as PbO, PbS, and SnO, are influenced by the contribution of lone pair-like *n*s electrons at the VBM,[60−64] so the role of analogous electronic states in BiCuOSe and BiCuOS was studied. The *n*s electrons of dianionic chalcogenides constitute core energy levels, but extend into the crystal lattice. These chalcogenide orbitals are visualized within the crystal structures of BiCuOSe and BiCuOS in Figure 10 using plots of the ELF, which permits visualization of the conditional probability of finding an electron in the vicinity of another electron of like spin.[65] The *n*s spheres around selenium and sulfur represent localization of these core electrons; the spherical shape consistent with s orbitals. The sphere around sulfur in BiCuOS is more localized than that around selenium in BiCuOSe. While this can be explained simply by the increase of the principal quantum number for the ns^2 electrons, it is also partly a result of the increased Cu 3d-Q *n*p orbital mixing as one proceeds down group 16 from S to Se. As the Cu-Q bond strengthens the electron density between the atoms increases and the *n*s electrons delocalize. The implications of this effect are observed in the measured conductivities of BiCuOSe and BiCuOS, where the enhanced conductivity of BiCuOSe can be attributed to higher hole mobility in the more hybridized, strongly covalent $(Cu_2Se_2)^{2-}$ layers.

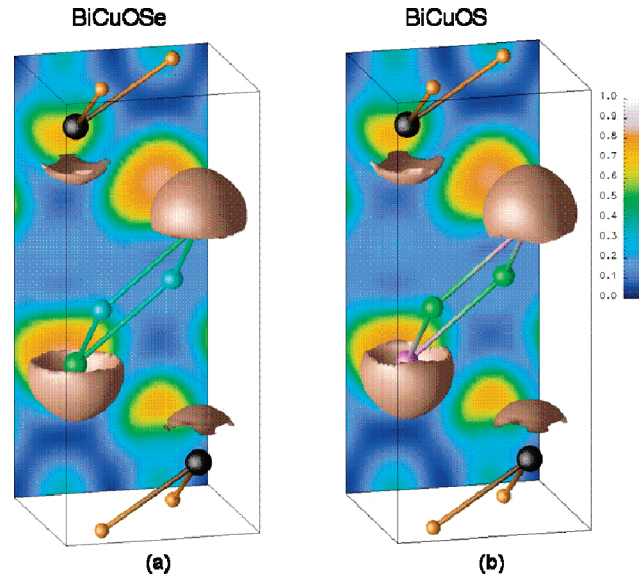

Figure 10. Crystal structures of (a) BiCuOSe (black spheres are Bi, orange O, Cu blue, and green Se) and (b) BiCuOS (black spheres are Bi, orange O, green Cu, and purple S). In the space of the structures, isosurfaces of the electron localization function (ELF) with a value of 0.84 are graphed around bismuth cations and chalcogenides anions. The map on the backend of the structure is the ELF, represented by color coding following the bar at the right. The deep blue end corresponds to poor localization and the white end to strong localization.

In contrast to the spherical *n*s orbitals of selenium and sulfur, the 6s orbitals of bismuth form lobes (Figure 10), indicating some p-orbital admixture. The question is whether the p character arises from mixing of s and p orbitals on the

(55) Hiramatsu, H.; Yanagi, H.; Kamiya, T.; Ueda, K.; Hirano, M.; Hosono, H. *Chem. Mater.* **2008**, *20* (20), 326–334.
(56) Hiramatsu, H.; Ueda, K.; Takafuji, K.; Ohta, H.; Hirano, M.; Kamiya, T.; Hosono, H. *J. Mater. Res.* **2004**, *19* (19), 2137–2143.
(57) Hiramatsu, H.; Orita, M.; Hirano, M.; Ueda, K.; Hosono, H. *J. Appl. Phys.* **2002**, *91* (91), 9177–9181.
(58) Ueda, K.; Hosono, H. *J. Appl. Phys.* **2002**, *91* (91), 4768–4770.
(59) Kamiya, T.; Ueda, K.; Hiramatsu, H.; Kamioka, H.; Ohta, H.; Hirano, M.; Hosono, H. *Thin Solid Films* **2005**, *486* (486), 98–103.
(60) Davis, J. L.; Riedl, H. R.; Schoolar, R. B. *Appl. Phys. Lett.* **1967**, *10* (10), 155–157.
(61) Joshi, R. K.; Durai, L.; Sehgal, H. K. *Phys. E* **2005**, *25* (25), 374–377.
(62) Pan, X. Q.; Fu, L. *J. Electroceram.* **2001**, *7* (7), 39–46.
(63) Watson, G. W. *J. Chem. Phys.* **2001**, *114* (114), 758–763.
(64) Watson, G. W.; Parker, S. C. *J. Phys. Chem. B* **1999**, *103* (103), 1258–1262.
(65) Seshadri, R. *Proc. Indian Acad. Sci., Chem. Sci.* **2001**, *113* (113), 487–496.

cation or whether it is the effect of covalency arising from cation s-anion p mixing. A similar case arises in α-PbO where the density of the Pb 6s and Pb 6p electronic states are well separated in energy, while O 2p states appear in the vicinity of the Pb 6s states. A positive Crystal Orbital Hamiltonian Population between O 2p and Pb 6s densities corresponds to a strongly covalent interaction, indicating that the p-orbital contribution to the Pb 6s lone pair originates from the anion rather than the metal cation.[65] Similarly, Seshadri and Hill have shown that a strong Bi−O COHP in the region of the Bi 6s states in monoclinic $BiMnO_3$ results in lobe-shaped Bi $6s^2$ lone pairs.[66] Therefore, since there is an overlap of O 2p states and Bi 6s states at approximately −11 eV (Figure 6), we postulate that the lobe shape of the bismuth valence orbitals in BiCuOQ results from a mixture of bismuth and oxygen states and in a strict sense the bismuth valence states cannot be regarded as a lone pair.

The overlap of Bi 6s and O 2p states at a low energy was unexpected, as many of the oxides and chalcogenides of Sn^{2+} ($5s^2$) and Pb^{2+} ($6s^2$), which have similar closed-subshell electronic configurations, exhibit *p*-type conductivities that benefit from mixing of the *n*s orbitals at the VBM. First-principle electronic structure calculations on these IV−VI rocksalt metal chalcogenides reveal that the metal cation *n*s-chalcogenide *n*p bonding states lie deep in the valence band and the antibonding states are high enough in energy to contribute to the VBM.[67−70] By increasing the number of available states for mobile holes to populate, this antibonding interaction at the VBM enhances the conductivity. It was therefore expected, in the case of BiCuOQ, that the bismuth 6s-chalcogenide *n*p antibonding states would contribute at the VBM, leading to a higher conductivity. As seen in Figure 6, instead of mixing with the selenium 4s orbitals at the VBM, the Bi 6s orbitals overlap with the O 2p orbitals and the antibonding states lay more than 2 eV deeper than the VBM. Hiramatsu et al. therefore recommend that ns^2-based cations should be coordinated only by chalcogenide ions in oxychalcogenides (and other mixed-ion compounds) to design an enhanced hole transport material.[55]

Conclusions

BiCuOSe was prepared by a hydrothermal reaction of Bi_2O_3, Cu_2O, Se, and hydrazine at a lower reaction temperature (250 °C) and time (48 h) than in previously reported solid state syntheses. A subtle balance between the solubilization of Bi_2O_3 and Cu_2O and the stabilization of monovalent copper and selenide was achieved by the selection of a reaction temperature of 250 °C. The measured conductivity of hydrothermally prepared BiCuOSe samples ($\sigma \approx 3.3$ S cm^{-1}) is greater than values reported for non-doped LnCuOS (Ln = La, Pr, Nd) and LaCuOSe samples and compares well with those of BiCuOS, CeAgOS, and CeCuOS. Owing to scalar relativistic effects associated with the large bismuth cations, the band gap is reduced ($E_g = 0.75$ eV), limiting its utility as a *p*-type transparent conductor.

Acknowledgment. The authors thank Professor R. Seshadri who contributed the theoretical calculations. We gratefully acknowledge support from the MRSEC program of the National Science Foundation (Grant DMR-0520513). Additional support was provided by the Department of Energy, National Renewable Energy Laboratory Subcontract (Award No. XAT-5-33636-02/DE-AC36-98GO) and Basic Energy Sciences (Award No. DE-FG02-08ER46536). This work was partially carried out in the frame of the STREP CoMePhS (NMP4-CT-2005-517039) supported by the European Community and by the CNRS, France. W.C.S. was additionally supported through a Chateaubriand postdoctoral fellowship and the Conseil Régional de Basse-Normandie. The SEM work was performed by Warefta Hasan in the EPIC facility of NUANCE Center at Northwestern University. NUANCE Center is supported by NSF-NSEC, NSF-MRSEC, Keck Foundation, the State of Illinois, and Northwestern University. We also thank Ms. Jill Millstone and Professor Chad A. Mirkin for the use of their UV-vis spectrometer and Julien Aubril and Sylvie Hebert for assistance with thermopower measurements.

Supporting Information Available: Figure S1 showing the EDX spectrum of the BiCuOSe. This material is available free of charge via the Internet at http://pubs.acs.org.

IC801267M

(66) Seshadri, R.; Hill, N. A. *Chem. Mater.* **2001**, *13* (13), 2892–2899.
(67) Payne, D. J.; Egdell, R. G.; Law, D. S. L.; Glans, P.-A.; Learmonth, T.; Smith, K. E.; Guo, J.; Walsh, A.; Watson, G. W. *J. Mater. Chem.* **2007**, *17* (17), 267–277.
(68) Togo, A.; Oba, F.; Tanaka, I.; Tatsumi, K. *Phys. Rev. B: Condens. Matter* **2006**, *74* (74), 195128/195121–195128/195128.
(69) Waghmare, U. V.; Spaldin, N. A.; Kandpal, H. C.; Seshadri, R. *Phys. Rev. B: Condens. Matter* **2003**, *67* (67), 125111/125111–125111/125110.
(70) Wei, S.-H.; Zunger, A. *Phys. Rev. B: Condens. Matter* **1997**, *55* (55), 13605–13610.